

University of Texas Rio Grande Valley

ScholarWorks @ UTRGV

Manufacturing & Industrial Engineering Faculty
Publications and Presentations

College of Engineering and Computer Science

11-2012

Droplet Spray Behavior of an Atomization-Based Cutting Fluid (ACF) System for Machining of Titanium Alloys

Chandra Nath

Shiv G. Kapoor

Anil K. Srivastava

The University of Texas Rio Grande Valley

Jon Iverson

Follow this and additional works at: https://scholarworks.utrgv.edu/mie_fac



Part of the [Industrial Engineering Commons](#), and the [Manufacturing Commons](#)

Recommended Citation

Nath, C, Kapoor, SG, Srivastava, AK, & Iverson, J. "Droplet Spray Behavior of an Atomization-Based Cutting Fluid (ACF) System for Machining of Titanium Alloys." Proceedings of the ASME 2012 International Mechanical Engineering Congress and Exposition. Volume 3: Design, Materials and Manufacturing, Parts A, B, and C. Houston, Texas, USA. November 9–15, 2012. pp. 2023-2033. ASME. <https://doi.org/10.1115/IMECE2012-88369>

This Conference Proceeding is brought to you for free and open access by the College of Engineering and Computer Science at ScholarWorks @ UTRGV. It has been accepted for inclusion in Manufacturing & Industrial Engineering Faculty Publications and Presentations by an authorized administrator of ScholarWorks @ UTRGV. For more information, please contact justin.white@utrgv.edu, william.flores01@utrgv.edu.

IMECE2012-88369

DROPLET SPRAY BEHAVIOR OF AN ATOMIZATION-BASED CUTTING FLUID (ACF) SYSTEM FOR MACHINING OF TITANIUM ALLOYS

Chandra Nath

University of Illinois at Urbana-Champaign
Urbana, IL, USA

Shiv G. Kapoor

University of Illinois at Urbana-Champaign
Urbana, IL, USA

Anil K. Srivastava

TechSolve Inc.
Cincinnati, OH, USA

Jon Iverson

TechSolve Inc.
Cincinnati, OH, USA

ABSTRACT

The aim of this research is to study droplet spray characteristics of an atomization-based cutting fluid (ACF) spray system including droplet entrainment angle and flow development regions with respect to three ACF spray parameters, viz., droplet and gas velocities, and spray distance. ACF spray experiments are performed by varying droplet and gas velocities. The flow development behavior is studied by modeling the droplets entrainment mechanism, and the density and distribution of the droplets across the jet flare. Machining experiments are also performed in order to understand the effect of the droplet spray behavior on the machining performances, viz., tool life/wear, and surface roughness during turning of a titanium alloy, Ti-6Al-4V. Experiments and the modeling of flow development behavior reveal that a higher droplet velocity and a smaller gas velocity result in smaller droplet entrainment angle leading to a gradual and early development of the co-flow with a smaller density and a better distribution of the droplet across the jet flare. Machining experiments also show that a higher droplet velocity, a lower gas velocity and a longer spray distance significantly improve the machining performances such as tool life and wear, and surface finish.

Key words: Titanium machining, Atomized droplets, Spray parameters, Co-flow jet, Machining performances.

NOMENCLATURE

K_x	Proportionality constant
N	Number of droplets
P_d	Static pressure in the droplet nozzle
P_{gs}	Static pressure of the gas at the jet center
S_d	Spray distance measured from the gas nozzle exit
U_d, U_g	Droplet and gas velocities, respectively

U_{gr}	Gas velocity at the outer contour of the gas jet
U_{gs}	Droplet velocity due to static pressure drop
U_{gx}	Local gas velocity
U_g	Resultant velocity of a co-flowing droplet
V_N	Control volume of the round nozzle
\dot{V}_f	Volumetric fluid flow rate
We	Weber number
K_y	Nondimensional group
d_g	Exit diameter of the gas nozzle
r_j	Local jet radius
r_p, r_i	Radius at the near-field and intermediate field regions
t	Time
θ_r	Droplet entrainment angle
θ_{js}	Droplet entrainment angle due to static pressure drop
ρ_f	Density of the cutting fluid
ρ_a	Density of the atmospheric air
ρ_d	Equivalent density of the droplet vapor

1. INTRODUCTION

Titanium alloys are being increasingly employed in a variety of engineering and biomedical applications due to their high specific strength, high-temperature strength, strong fracture and corrosion resistance, and biocompatibility. However, during machining of these alloys, high cutting zone temperature (above 500 °C) localized in the vicinity of the cutting edge, and poor thermal conductivity and strong chemical affinity of titanium impose many constraints that accelerate tool wear [1-8].

Researchers have applied high-pressure cooling (HPC) and cryogenic cooling and observed tool life improvement over conventional flood cooling [2-9]; however, these processes do not offer the productivity by the same order due to significantly

higher consumption of cutting fluid and/or energy [6-9]. Recently, Nath *et al.* [10] designed and evaluated an atomization-based cutting fluid (ACF) spray system for turning of a titanium alloy Ti-6Al-4V. By employing the ACF spray system, they observed an improvement in tool life of about 40-50% over flood cooling. A combination of spray system parameters including flow rate (20 ml/min), high-pressure gas (~10.3 bar), spray distance (35 mm), impingement angle (35°), and air-CO₂ gas mixture improved machining performances such as tool life, cutting force, and chip breakability. It was also seen that the air-CO₂ mixture enhanced chip breakability due to its lower initial dispensing temperature. However, the effects of other ACF spray parameters were not deeply understood. While such an ACF spray system appears to be favorable, there is a lack of a physics-based understanding of the phenomena underlying the droplet spray behavior with respect to these ACF spray parameters.

In ACF spray system, two coaxial nozzles of different diameters are used for dispensing the droplets of cutting fluid towards the cutting zone [10-15]. Micro-size fluid droplets that are produced by an ultrasonic atomizer flow through the coaxial outer nozzle (named 'droplet nozzle') at a low velocity, and are entrained by the high-velocity gas flowing through the inner nozzle (called 'gas nozzle') to produce a focused axisymmetric droplet jet. During machining, the center of the ACF spray jet is directed towards the cutting region in order to obtain its maximum momentum, which is important for effective cooling and penetration at the tool-chip cutting interface. Therefore, the center of the jet has to be fully-developed with the droplets being distributed uniformly into the gas before it impinges at the cutting zone. The centerline mixing behavior with respect to the spray distance of such a co-flow spray jet can be influenced by the velocity of the droplet particles and the high-velocity gas that in turn influences the film formation behavior, and is likely to dominate machining performances. While the previous studies [16-19] provide valuable insight into co-flow spray jets produced from two gases, the velocity of the outer co-flow gas was not varied. Also, the entrainment mechanism of the outer gas into the inner gas was not studied. Rukosuyev *et al.* [11-12] observed droplet spray behavior such as focus height and length at different combinations of gas and droplet velocities for micromachining experiments. However, attention was not given to describe the flow development between the droplets and the gas due to entrainment/diffusion and the ACF spray parameters.

The objective of this research is to study droplet spray characteristics such as droplet entrainment zone and flow development regions with respect to three ACF spray parameters including droplet and gas velocities, and spray distance. In regard to this, ACF spray experiments are performed by varying droplet and gas velocities, and the droplet-gas flow development characteristics such as droplet density and distribution are observed with respect to spray distance. The flow development behavior for an ACF spray system is modeled in order to understand the entrainment mechanism of the droplets, and the density and distribution of

the droplets across the jet flare. Machining experiments also are performed in order to understand the effect of the droplet spray behavior on the machining performances, viz., tool life/wear, and surface roughness during turning of Ti-6Al-4V.

The rest of the paper is organized as follows. Section 2 describes ACF spray experiments, and observations of the droplet entrainment angle, and density and distribution with respect to the ACF spray parameters. In Section 3, modeling of ACF droplet spray characteristics was presented in order to theoretically understand the droplet spray characteristics. Section 4 deals with setup and procedure for Ti-6Al-4V turning experiments, and the effect of droplet spray behavior on the machining performances. Section 5 draws conclusions based on the theoretical and the experimental findings.

2. ACF SPRAY EXPERIMENTS

The ACF spray experiments were conducted using the spray unit shown in Fig. 1. The system consists of: i) an ultrasonic vibration-based atomizer; ii) cutting fluid reservoir with a delivery tube; iii) nozzle unit; iv) high-pressure gas delivery nozzle/tube at the nozzle-spray unit; and v) four low-velocity air delivery tubes placed behind the atomizer tip. The atomizer (Model VC5040AT, Sonics and Materials, Inc.) produces a mean droplet size of 50 μm at the maximum flow rate of 166.67 ml/min. Once the fluid is atomized, the micro-size droplets move forward to the nozzle unit that consists of coaxial outer droplet and inner gas nozzles. The exit diameters of the droplet nozzle and the high-velocity gas nozzle are designed to be 18.8 mm and 1.6 mm, respectively. Both nozzles are considered to have a convergence slope of 4° and 0.75°, respectively, and the inner gas nozzle was placed 5 mm inside the droplet nozzle exit position in order to avoid divergence of droplets [10-12].

Experiments using a 2² factorial design considering two droplet velocities and two gas velocities were performed to study the effects of droplet velocity and gas velocity on droplet spray characteristics including droplet entrainment zone (e.g. angle and distance) and flow development regions described by the droplet density and distribution. Droplet velocities were chosen to be 0.2 and 1.2 m/s. Note that, the droplets at a velocity of larger than 1.5 m/s that are within the favorable range suggested by Rukosuyev *et al.* [11]. Gas velocities were selected to be 26 and 36 m/s (10.3 bar and 20.6 bar, respectively, when measured by an anemometer). Spray distance, which is another ACF spray parameters in this study, will also be discussed in regard to flow development region. The fluid flow rate was chosen to be 20 ml/min.

Figures 2(a)-(d) depict photographs of four different combinations of droplet velocity, U_d and gas velocity, U_g for an ACF spray system. The droplet entrainment angle, θ_r , the direction at which the outer co-flow fluid droplets converge towards the center axis for conditions (a)-(d) are measured to be about 43.26°, 24.44°, 55.0°, and 29.05°, respectively. It is observed that when droplet velocity increases (conditions (a) vs. (b) or (c) vs. (d)), the droplet impingement angle, θ_r becomes

smaller. A smaller value of θ_r allows droplets to be entrained slowly with a comparatively longer downstream distance resulting in a larger droplet entrainment zone. Moreover, with the increase in gas velocity (conditions (a) vs. (c) or (b) vs. (d)), the droplet entrainment angle increases leading to a smaller droplet entrainment zone.

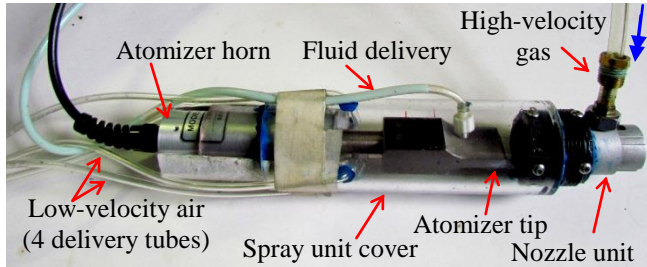


Figure 1 – Photograph of the ACF spray unit [10].

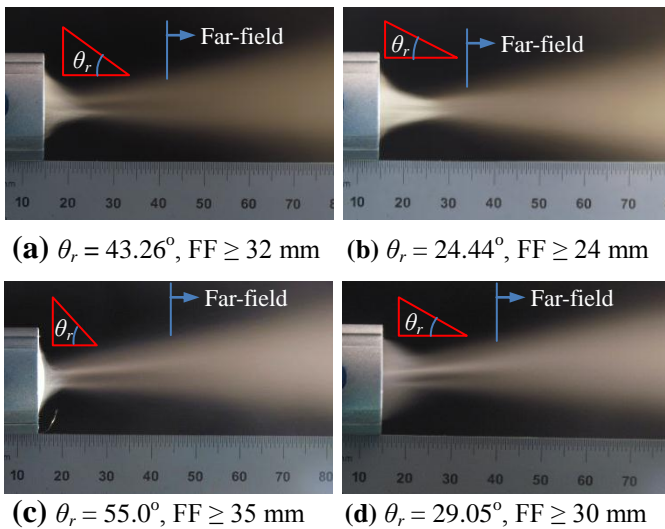


Figure – 2 Photographic images of ACF droplet-gas co-flow at: (a) $U_d = 0.2$ m/s, $U_g = 26$ m/s; (b) $U_d = 1.2$ m/s, $U_g = 26$ m/s; (c) $U_d = 0.2$ m/s, $U_g = 36$ m/s; (d) $U_d = 1.2$ m/s, $U_g = 36$ m/s (scale: mm; Gas nozzle exit is located at reading ‘10’).

It can also be seen that each of the ACF spray conditions produces a droplet-free zone at the center of the nozzle. Depending on the spray condition, the droplet and the gas merge after a certain distance where the droplets are observed to be distributed uniformly across the jet flare. Photographic images provided by Rukosuyev *et al.* [11-12] also demonstrated a separation between the center gas jet and the droplet. Such a flow development behavior can be represented by a schematic diagram shown in Fig. 3. As seen in figure, as soon as the gas exits at the center, it entrains the surrounding fluid droplets creating a converging droplet entrainment zone around the gas nozzle for a certain distance. The resultant droplet-gas jet then diverges, but the mixing or flow development continues. The entire flow development region beginning from the gas nozzle

exit point can be described by three distinct regions: near-field (NF), intermediate-field (IF), and far-field (FF). These are usually characterized by a normalized axial position, x/d_g , where d_g is the exit diameter of the gas nozzle [20, 21]. Typical cross-sections A-A, B-B, and C-C of the jet flare at the NF, IF, and FF regions, respectively, are schematically illustrated in Fig. 3. In the NF region, a potential core is observed with absence of the outer co-flow medium. On the other hand, in the FF region, no potential core is observed as the mixing is fully-developed (i.e. ‘self-similar’ state) and hence, the droplets are uniformly distributed throughout the jet flare. The IF or transition region that lies between these two regions contains a few droplets as it approaches to the FF region. Note that the entrainment between the resultant jet and the ambient air at the outer contour can occur; however, this secondary entrainment is not discussed here because the droplet spray behavior at the center is of main interest during machining.

When considering a liquid dispensing into still ambient air or parallel moving air/gas, the authors in [20-21] found that the FF region is approximately $x/d_g \geq 25$. In this study, since the exit diameter of the inner gas nozzle is set 1.6 mm, the self-similar state (i.e. distance between the gas nozzle exit and the FF region) is expected to fall at 40 mm or beyond. However, as seen in Figs. 2(a)-(d), the fully-developed or FF region is estimated to be in a range of approximately 24-35 mm for the conditions observed, which is smaller than the usual axisymmetric jet studies [20-21]. The early flow development of the self-similar state in the present study may be due to the fact that the density of the center gas (air) is lower than the outer co-flow gas (droplet). It is also observed from Figs. 2(a)-(d) that when gas velocity decreases, the distance between the gas nozzle exit and the FF region becomes smaller. Thus the downstream distance for the self-similar state, where the flow becomes asymptotic, is smaller for a lower gas velocity. Similar observation was also reported in co-flow studies in [17].

From the above experiments, it is clear that droplet and gas velocities in an ACF spray system influence the droplet entrainment mechanism and the droplet-gas mixing behavior into the center jet. A combination of a higher droplet velocity (1.2 m/s) and a lower gas velocity (26 m/s), among four spray conditions observed, provide the best spray condition in term of droplet entrainment angle. Also, the self-similarity characteristic, which is relevant to the ACF spray distance, was observed to be formed earlier for this spray test than for the other three tests. The following section will present a model that describes how the three ACF spray parameters influence the flow development characteristics in an ACF spray system. Moreover, theoretical relationship of droplet and gas velocities with droplet entrainment angle and entrainment zone, and their influence on droplet density and distribution across the jet flare at three different regions (i.e. NF, IF, and FF) will be presented.

3. MODELING OF ACF DROPLET SPRAY BEHAVIOR

When a high-velocity fluid is dispensed into a still atmospheric air or to a low-velocity parallel moving fluid,

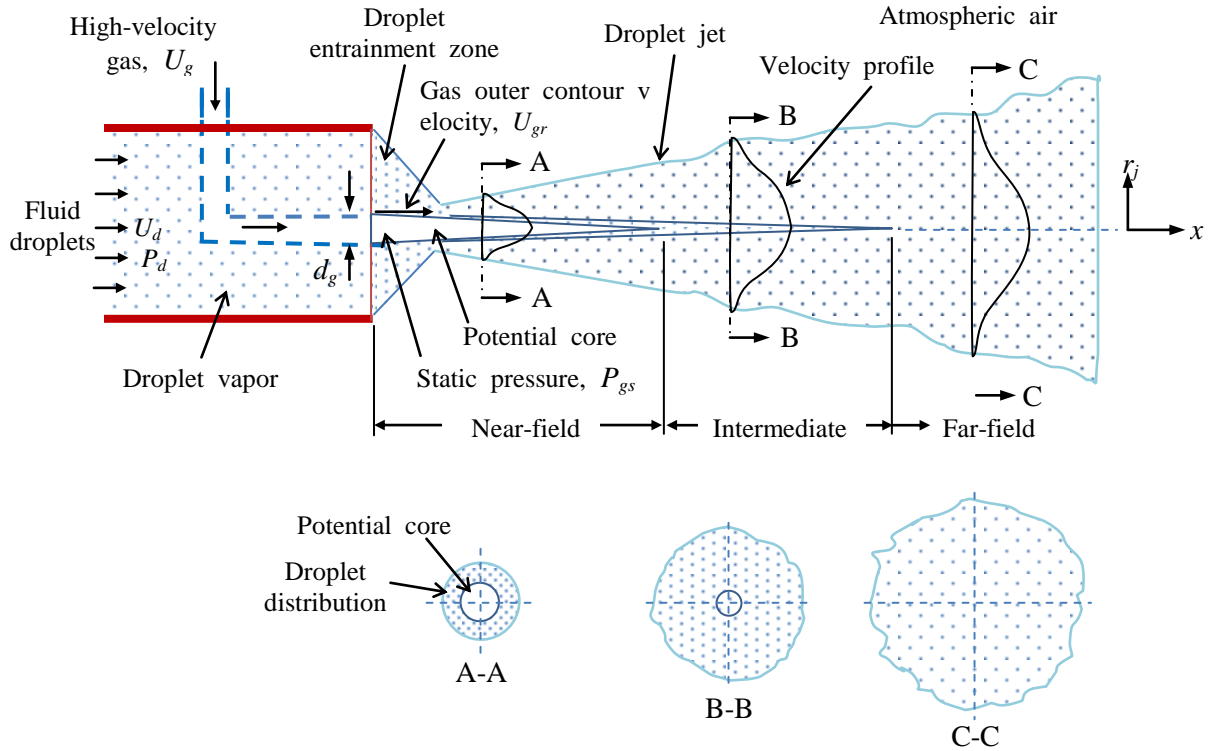


Figure – 3 Schematic of a typical axisymmetric co-flow jet produced by a high-velocity gas and fluid droplets, and its flow evolution regions with respect to downstream position. (A-A, B-B, and C-C denote cross-sections at three different regions).

entrainment of the outer fluid into the inner fluid takes place [16-23]. As the high-velocity fluid jet flows at a dynamic pressure, its static pressure reduces according to Bernoulli's principle [24]. This causes a pressure difference between the jet domain and the surrounding fluid/air. Moreover, if a compressible fluid like gas is dispensed (exit from a nozzle), it immediately expands in the radial direction. The pressure difference and the gaseous nature of the dispensing fluid cause entraining the outer surrounding gas or air to flow in and mix with the center gas. Due to differences in fluid properties and flow dynamics between the center jet and the outer droplets, one fluid diffuses into the other and vice versa. The slow-moving droplets cause aerodynamic drag to the high-velocity gas that results in deceleration of the gas, and the momentum lost by the high-velocity gas is received by the droplets [22]. Their momentum gradually evolves to an equilibrium state (i.e. fully-developed) as the jet moves forward. As a result, the velocity or dynamic pressure of the center jet, which is usually assumed to follow a Gaussian profile [20, 23, 25], gradually decays with respect to the downstream position (Fig. 3).

In this section, the droplet entrainment angle with respect to droplet velocity, gas velocity, and the density and distribution of the droplets across the jet flare at three different flow development regions will be modeled. In order to estimate the droplet entrainment angle, the following assumptions are made about the nature of the droplets:

- i) Fluid droplets inside the droplet nozzle uniformly mix with the ambient air and create a homogenous droplet vapor. It appears to be a single gaseous phase, but different from the centerline gas jet in nature;
- ii) Fluid droplets do not interact each other during flow (non-condensing);
- iii) The fluid droplets are uniform in size;
- iv) Gravitational force acting on the droplets is ignored.

3.1 Droplet Entrainment Angle

When a high-velocity gas is dispensed from a nozzle, the pressure difference between the jet and the surrounding rest or co-flow jet increases with the increase in its velocity. Gaussian mean velocity profile in Fig. 3 suggests that the velocity or dynamic pressure of the jet is the largest at the center producing to the least static pressure. In ACF spray system, the velocity of a static single droplet, U_{gs} towards the jet center due to reduced static pressure can be calculated from Bernoulli's principle,

$$P_d - P_{gs} = \frac{1}{2} \rho_d U_{gs}^2, \quad (1)$$

where, P_d, P_{gs}, ρ_d are static pressure of the droplets in the droplet nozzle, the static pressure of the gas at the jet center, droplet equivalent density of the droplet vapor, respectively. The pressure difference, $(P_d - P_{gs})$ can be directly measured from a piezometer. The static pressure at the jet center, P_{gs} decreases with an increase in gas velocity. For a given control

volume consisting of a circular ACF nozzle unit (see Fig. 1), an equivalent density of the droplet vapor can be calculated using mass conservation law:

$$\rho_d = \frac{\rho_f \dot{V}_f t + \rho_a (V_N - \dot{V}_f t)}{V_N}, \quad (2)$$

where, ρ_f and ρ_a are the fluid and air density, \dot{V}_f is the volumetric fluid flow rate, t is time, V_N is the control volume in round nozzle.

Now, let a single droplet is entrained in the droplet entrainment zone, which is formed around the potential core immediately after the gas nozzle exit. When the droplet approaches to flow into the center at an angle, θ_{gs} due to the static pressure drop, the dynamic pressure of the jet that flows at a high velocity, U_g pulls off the droplet in its flow direction at a velocity, U_{gr} at the outer contour of the jet. The flow of the droplet due to the velocities, U_d , U_{gs} , and U_{gr} can be represented by a velocity diagram illustrated in Fig. 4. The resultant droplet entrainment angle, θ_r of a co-flowing droplet can be expressed as:

$$\theta_r = \tan^{-1} \left(\frac{U_{gs}}{U_d + U_{gr}} \right), \quad (3)$$

where U_{gr} is the velocity at the outer contour of the jet, and its value is obtained as:

$$U_{gr} = k_x U_{gx}, \quad (4)$$

where, k_x is a proportionality constant, and U_{gx} is the local jet velocity in the x-axis. At the nozzle exit, $x = 0$, the value of U_{gx} is approximately equal to U_g ; however, it decreases with the increase in downstream distance as the velocity of the jet decays [20, 23, 25]. Also, for a compressible non-viscous fluid flow, $k_x \approx 1$ at $x = 0$, because the velocity at the jet center is almost equal to the velocity at the outer contour [21, 26].

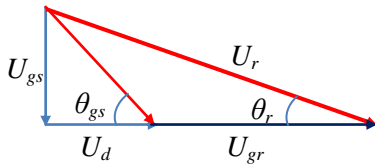


Figure – 4 A typical velocity diagram for a single droplet in the droplet entrainment zone (U_r : resultant velocity).

Equation 3 states that the droplet entrainment angle can be influenced by both gas velocity and droplet velocity. A higher droplet velocity, U_d governs a droplet to follow at a smaller angle, θ_r with respect to the jet axis. However, the dependence

of gas velocity, U_g on the value of θ_r is a bit complex. With the increase in gas velocity, U_g , both the values of U_{gr} and U_{gs} increase. Note that, if the value of U_g (or dynamic pressure) of the jet increases, the value of U_{gs} also increases due to a comparatively larger static pressure drop, $(P_d - P_{gs})$. Thus, it is hard to predict the influence of U_g without knowing the value of the static pressure of the jet, P_{gs} .

The expression for the droplet entrainment angle, θ_r in Eqn. (3) is obtained considering a single droplet in the droplet entrainment zone. However, when considering a number of droplets as ambient gas around the center jet, the droplet that is close to the gas jet contour will move faster than the one that is further away. Therefore, the value of θ_r estimated from the above relationships for a co-flow jet may not be accurate.

3.2 Droplet Density and Distribution across Jet Flare

As described in Section 2, the density and distribution of droplets across the jet flares at locations A, B, and C for three different regions: NF, IF and FF, respectively, are observed to be different (Fig. 3) due to gradual mixing between the droplets and the gas with respect to the downstream distance. Across the jet flare at cross-section A-A, the resultant jet of the droplets and the gas does not significantly diverge. Also, the diffusion between the droplets and the gas does not happen that much. As a potential core (i.e. no presence of the droplets) is distinctly observed at the center and the combined jet has a smaller outer contour, the number of droplets for a given volume (i.e. droplet density) becomes too high. On the other hand, across the jet flare at C-C, the diffusion is fully-developed, and the jet contains a larger contour because of divergence. As a result, the droplets uniformly distribute and the droplet density becomes smaller. At the cross-section B-B, the number of droplets across the jet flare may not be significant, but the size of potential core becomes smaller. If for the locations A, B, C, a small length, Δx is considered in both directions along x-axis, the average droplet density across the jet at the respective locations can be estimated as:

$$\rho_{dA} = \frac{N}{2\pi \Delta x (r_{jA}^2 - r_{pA}^2)} \quad (5a)$$

$$\rho_{dB} = \frac{N}{2\pi \Delta x (r_{jB}^2 - r_{iB}^2)} \quad (5b)$$

$$\rho_{dC} = \frac{N}{2\pi \Delta x r_{jC}^2}, \quad (5c)$$

where, N is the number of fluid droplets depending on the flow rate and atomizer frequency, r_{jA} , r_{jB} , r_{jC} are radii of the jet boundary layer at the locations A, B, C, respectively, and r_{pA} , r_{iB} are radii of the potential core and the intermediate core at the locations, A, B, respectively. Note that the jet boundary layer suffers from an eddy (turbulence) effect due to

entrainment of atmospheric air [20-23]. As such, average values of η_{jB} and η_{jC} should be taken for the intermediate and far-field regions. Eqns. 5(a)-(c) suggest that the average droplet density is significantly high at location A followed by medium at location B, and the least at location C.

3.3 Condensation due to Multiple Fluid Droplets

Developing the relationships for droplet density and distribution in Section 3.2, it was assumed that the droplet vapor that consists of air and droplets behave like one medium as a non-condensing gas. However, the fluid droplets may interact, especially when they come close or touch each other. This situation can take place in two ways: during entrainment in the droplet entrainment zone and during mixing within the NF (i.e. near-field) region. For a set of droplet and gas velocities, if the droplet entrainment angle increases, then the size droplet entrainment zone decreases due to a smaller downstream distance. In such a case, droplet density becomes higher that may lead to decrease in inter-droplet distance. If two or more droplets touch each other, they will result in condensation and will form, comparatively, a larger droplet. Also, during mixing within the NF region, the entire amount of droplets usually pass through a smaller jet flare (for example, at cross section A-A in Fig. 3) if the droplet entrainment angle increases. As the droplets again become closer, there is a higher chance of getting them closer that will lead to a condensation effect. If the droplet size becomes larger, it will influence film formation behavior [10, 15], and hence will affect the cooling and lubrication characteristics during machining.

In order to avoid condensation of the fluid droplets in the entrainment zone and next in the mixing region (i.e. near-field and intermediate-field), it is preferable to allow the droplets to be entrained slowly and gradually until the intermediate region. In such a case, the radius of the jet at the NF and the IF regions will increase and the droplet density will decrease that will protect the fluid droplets from condensation. Figures 5(a)-(b) illustrate schematic diagrams for a smaller and a larger droplet impingement angles, respectively. A smaller droplet entrainment angle leads to increase the size of the droplet entrainment zone as well as the radius of the droplet-gas resultant jet, η_j . Using Eqn. (5a), it can be seen that the average droplet density for a larger value of θ_r (say, θ_{r1}) at the same location A of the potential core will be higher than that for a smaller value of θ_r (say, θ_{r2}). That means, if $\theta_{r1} > \theta_{r2}$, then $\rho_{d1} > \rho_{d2}$ since $\eta_{j1} < \eta_{j2}$. This condition can be achieved by controlling the gas velocity and the droplet velocity that control the droplet entrainment angle (Eqn. (3)). Note that during machining with ACF spray system, the center of the jet is directed towards the cutting zone. As such, a fully-developed flow is required in order to produce a uniform fluid film for penetrating into the tool-chip interface. In Section 4, the machining experiments are conducted to understand the influence of the droplet spray behavior on the tool-chip interface and the resulting machining performances viz., tool life and wear, and surface roughness.

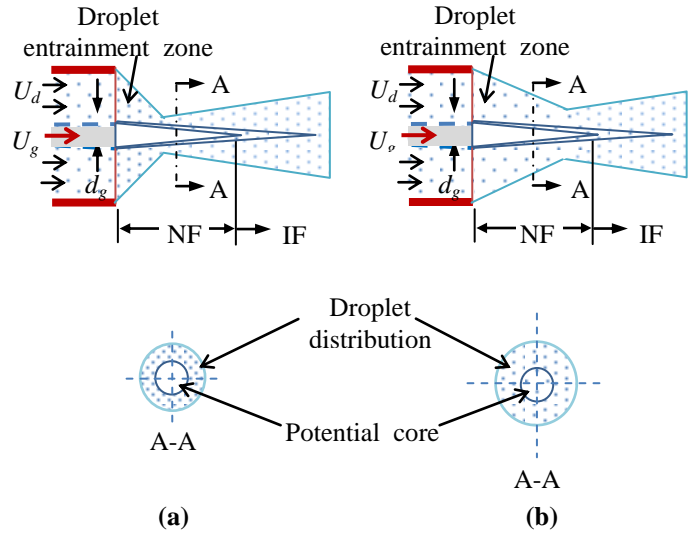


Figure – 5 Variation of the droplet density across the jet flare at the same location A for: (a) smaller; and (b) larger droplet entrainment angles.

4. TI-6AL-4V TURNING EXPERIMENTS

4.1 Experimental Setup and Design

A schematic of an ACF spray system setup for turning operation is shown in Fig. 6(a). A *Mori Seiki Frontier L-1* CNC lathe was used for turning experiments as depicted in Fig. 6(b). A cylindrical Ti-6Al-4V bar of size $\text{Ø}175 \text{ mm} \times 325 \text{ mm}$ was used for turning. Uncoated microcrystalline carbide inserts ISO grade K313 from *Kennametal* was used as tool material and placed on a standard *Kennametal* shank. The tool geometry was set as follows: 5° rake angle, 11° clearance angle, 60° major cutting edge angle, 0.8 mm nose radius. The tool shank was secured with a *Kistler* 3-component force dynamometer (type 9121) to capture the cutting force data through a *National Instrument* data acquisition system (SCB-68) integrated with the *LabVIEW* software. The cutting conditions were selected to be 80 m/min cutting speed, 0.2 mm/rev feed rate, and 1 mm depth of cut [2-8]. Water-soluble cutting fluid S-1001 at 10% dilution was used as coolant at a flow rate of 20 ml/min. The thermo-physical properties of 10% S-1001 is as follows: density 1003 kg/m^3 , surface tension 41 mN/m, viscosity 1.22 cP, and thermal conductivity 0.53 W/m-K .

The ACF spray unit shown in Fig. 1 was used in the present study. The unit was placed inside the machine on a metal frame that is fastened with the lathe turret. The frame allows the ACF spray unit to be adjusted at a desired impingement angle, orientation, and spray and spot distances. The spray unit was directed on the tool rake face and its centerline was oriented along the major cutting edge (i.e. 60° with the work axis) for impinging the droplets in the direction of the cutting edge. The spot distance (see Fig. 1) is set about 8 mm. As a train of droplets impinged, a fluid film continuously produces and moves forward that penetrates into the tool-chip interface. Before impinging on the rake face, the distribution and the

density of the droplets across the jet flare at different axial position of the jet are influenced by three system parameters, viz., gas velocity, atomized droplets velocity, and spray distance. A replicated 2^3 full factorial design was used in conducting experiments as seen in Table 1. The gas velocity was chosen to be 26 m/s and 36 m/s (measured by a handheld digital anemometer (from *Omega*) at 10.3 bar at 20.6 bar, respectively), and the impingement angle was chosen to be 35° so that the spreading regime (nondimensional Weber number, $We \geq 10$ and group, $K_y \leq 17$) occurs on the rake face [13]. Air-CO₂ mixture was used as the high-velocity gas for controlling a lower initial dispensing temperature of about 1-2 °C [10].

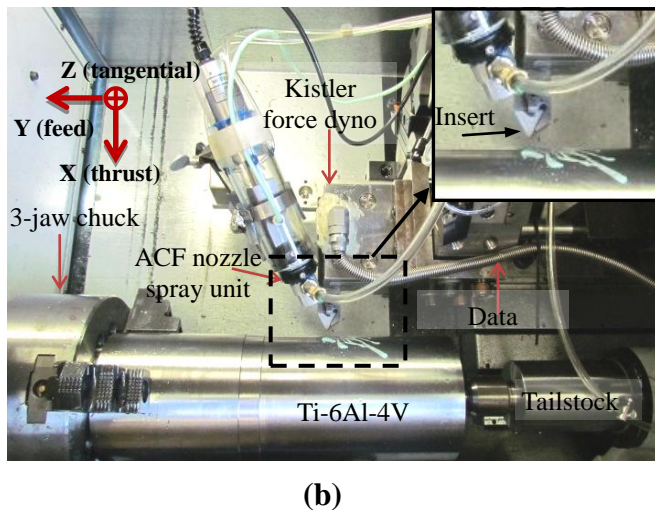
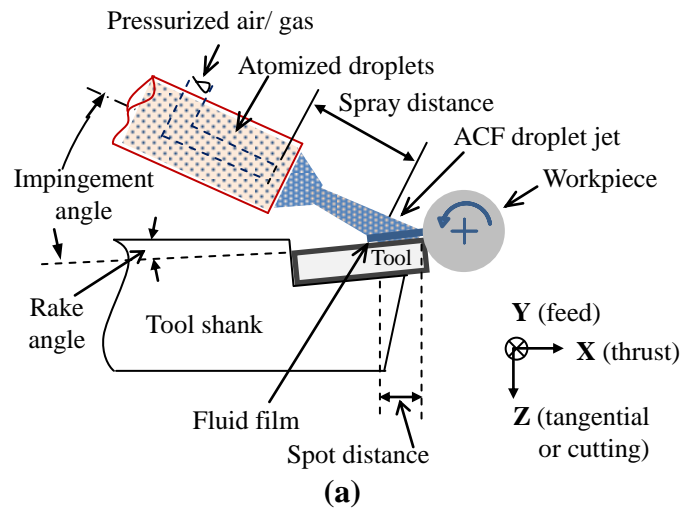


Figure 6 – (a) ACF spray parameters in turning setup; (b) Experimental setup with the ACF spray system in a CNC lathe (inset: cutting insert).

For all the cutting conditions, the tools were removed from the setup first at 4 min and then at 6 min to observe the progress of wear. The tool thereafter was checked every one minute until the maximum flank wear land reached 0.6 mm according to the

ISO standard. The maximum tool flank wear was measured using a *Quadra-Check 300* optical microscope. Average and maximum surface roughness (R_a and R_z , respectively) values were measured using a portable roughness tester *TR 100*. The surface roughness was measured starting at 1 min with an interval of 2 min until the tool survives.

Table 1 Factor levels for the ACF spray parameters.

Parameters	Low (-)	High (+)
(x_1) Droplet velocity, U_d (m/s)	0.2	1.2
(x_2) Gas velocity, U_g (m/s)	26	36
(x_3) Spray distance, S_d (mm)	25	35

4.2 Results of the Turning Experiments

In this section, the experimental results of the effects of the ACF spray parameters, viz., droplet velocity, gas velocity, and spray distance on the machining performances including tool life/wear, and surface roughness are presented.

4.2.1 Tool Life and Wear

Turning tests on Ti-6Al-4V were performed using the ACF spray system for the conditions listed in Table 1. Table 2 depicts tool life for two repeated test runs and their average value for each set of ACF spray conditions. An analysis at 95% confidence interval show that the tool life is significantly influenced by all three spray parameters such as spray distance, droplet velocity, and gas velocity. With the increase in spray distance and droplet velocity, and the decrease in gas velocity, regardless of varying them individually or together, the tool life can undoubtedly be improved during titanium machining.

Table 2 – Tool life at different ACF spray conditions.

Test no.	Parameters			Tool life (min)		
	x_1	x_2	x_3	Run 1	Run 2	Average
1	0.2	26	25	7	7	7
2	1.2	26	25	8	8	8
3	0.2	36	25	7	8	7.5
4	1.2	36	25	8	7	7.5
5	0.2	26	35	9	8	8.5
6	1.2	26	35	10	11	10.5
7	0.2	36	35	9	8	8.5
8	1.2	36	35	10	9	9.5

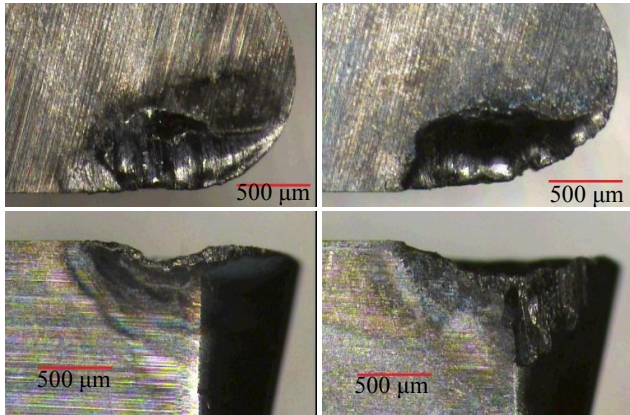
The effect of spray distance, S_d on tool life can be observed by typical wear of the tool rake and flank shown in Figures 7 and 8 for Test nos. 2 and 6, respectively, where the values of droplet and gas velocities are kept constant (U_d : 1.2 m/s, U_g : 26 m/s). It is seen that when spray distance, S_d

increases from 25 to 35 mm, the tool survives for longer time. The maximum tool flank wear widths for these two tests are measured to be about 0.193 and 0.153 μm at 4 min, 0.721 and 0.453 μm at 8 min cutting, respectively. Also, an improved tool rake face condition can be observed for 35 mm as compared to that for 25 mm spray distance.

The tool life improvement at 35 mm spray distance is due to the fact that, the droplets-gas co-flow is fully-developed (i.e. in the FF region) in all the ACF conditions tested in Figs. 2(a)-(d). The fluid droplets across the jet flare are distributed uniformly across the jet flare, as seen in Fig. 3. As such, an even and thicker fluid film continuously forms that leads to a better cooling and lubrication effect at the tool-chip cutting interface. Since the center of the spray jet is directed towards the cutting zone during turning, this fluid film results in longer tool life. In contrast, since the fluid droplets at the center of the jet before the FF region are comparatively less, the resultant fluid film becomes uneven and much thinner. Such a fluid film may not provide enough cooling and lubrication effects, and thus cause

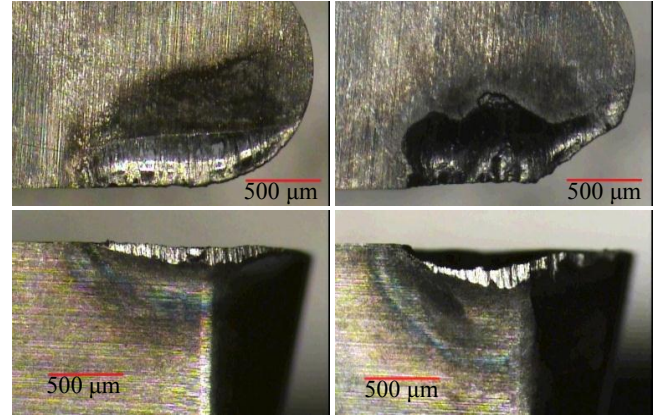
increased tool wear.

The effect of variation of droplet velocity from 0.2 to 1.2 m/s can be observed by images of tool rake and flank wear in Figs. 7 and 9, for example, where gas velocity (26 m/s) and spray distance (25 mm) are kept fixed. It is found that the tool wear decreased with the increase in droplet velocity. According to Eqn. (3), if droplet velocity, U_d increases, the droplet entrainment angle, θ_r becomes smaller. Also, as seen in ACF spray experiment in Figs. 2(a)-(b), if droplet velocity increases from 0.2 to 1.2 m/s at the same gas velocity of 26 m/s, the value of θ_r decreases from 43.26° to 24.44° . Similar trend is observed in Figs. 2(c)-(d) at another gas velocity of 36 m/s. A smaller value of θ_r allows gradual mixing or diffusion of the droplets into the gas jet. As a result, the droplet density becomes lower (see Eqns. 5(a)-(c)) and condensation between the droplets can be avoided (see Section 3.3). Also, this condition helps in early development of the FF region (in Fig. 2(b)) that helps in achieving an improved tool life as compared to the other conditions.



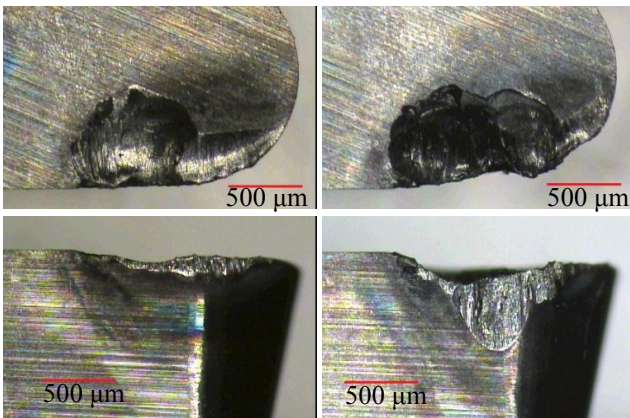
(a) at 4 min (b) at 8 min

Figure – 7 Photographs of tool rake and flank faces for Test no. 2 (U_d : 1.2 m/s, U_g : 26 m/s, S_d : 25mm).



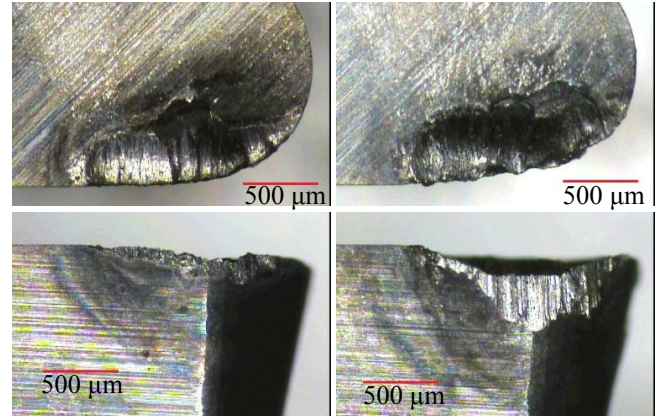
(a) at 4 min (b) at 8 min

Figure – 8 Photographs of tool rake and flank faces for Test no. 6 (U_d : 1.2 m/s, U_g : 26 m/s, S_d : 35mm).



(a) at 4 min (b) at 7 min

Figure – 9 Photographs of tool rake and flank faces for Test no. 1 (U_d : 0.2 m/s, U_g : 26 m/s, S_d : 25mm).



(a) at 4 min (b) at 8 min

Figure – 10 Photographs of tool rake and flank faces for Test no. 8 (U_d : 1.2 m/s, U_g : 36 m/s, S_d : 35mm).

Figures 8 and 10 show images of tool rake and flank faces at different gas velocities for Test nos. 6 (U_g : 26 m/s) and 8 (U_g : 36 m/s), where droplet velocity (1.2 m/s) and spray distance (35 mm) are kept constant. With the increase in gas velocity, the tool life shortens. From the ACF spray experiments in Figs. 2(a) and (c), it is found that with the increase in gas velocity from 26 to 36 m/s at the same droplet velocity of 1.2 m/s, the value of θ_r increases from 43.26° to 55.0°. Figures 2(b) and (d) also show similar trend. This reveals that a larger gas velocity results in larger droplet entrainment angle, θ_r . As a result, the droplet density and distribution change in a way that it adversely influences tool life (Test nos. 6 and 8).

In summary, a larger spray distance (35 mm), a higher droplet velocity (1.2 m/s), and a smaller gas velocity (26 m/s) enhances tool life by reducing tool wear in titanium machining.

4.2.2 Surface Roughness

Figures 11(a) and (b) present the average and maximum roughness values at different cutting intervals for the conditions under the same Test nos. 1, 2, 6, and 8 that were discussed in Section 4.2.1. It is observed that the surface degraded as the tool wear progresses with the cutting time. However, depending on the ACF spray conditions, the roughness values become different after 3 min cutting time. With the increase in spray distance and droplet velocity, and the decrease in gas velocity, the increment in surface roughness values is gradual and found to be comparatively smaller. The tool in Test no. 6 operated at a larger spray distance (35 mm), a higher droplet velocity (1.2 m/s), and a lower gas velocity (26 m/s) offered improved surface roughness compared to the other three tests. In contrast, the roughness values in Test no. 1, which is conducted at 25 mm spray distance, 0.2 m/s droplet velocity, and 36 m/s gas velocity, increases at a considerably higher rate. This finding is in agreement with the earlier observations on tool life and wear.

In order to understand the effect of the spray behavior on

both tool wear and surface finish, the three cutting force components, viz., tangential, feed and thrust forces were collected. Table 3 presents the values of these force components and their resultant cutting force at different cutting intervals until the tool life for Test nos. 1, 2, 6 and 8 (refer to Table 2 and Figs. 7-10). Also, in order to understand the penetration and lubrication effect of ACF spray-produced thin film at the tool-chip cutting interface, cutting force data at these intervals are represented in terms of friction coefficient. Figure 12 presents values of friction coefficient, μ that is calculated using the following expression [7],

$$\mu = \frac{F_z \sin \phi \tan \gamma_o + F_y \cos \gamma_o}{F_z \sin \phi \cos \gamma_o - F_y \sin \gamma_o} \quad (6)$$

where, F_y , F_z , ϕ , γ_o are feed force, tangential cutting force, principle cutting edge angle, and orthogonal rake angle, respectively.

When increasing spray distance from 25 to 35 mm (Test nos. 2 and 6, respectively) with other two spray parameters remain constant, the values of the cutting forces and the friction coefficient are found to be comparatively lower. This is because, at a spray distance of 35 mm, the fluid droplets are found to be distributed uniformly across the jet flare (see Figs. 2(a)-(d)). This causes to forming an even and uniform fluid film that helps in penetrating into the tool-chip cutting interface. This helps in achieving a better cooling and lubrication effect, and thus enhances tool life and surface roughness in this spray condition. In contrast, at a smaller spray distance, the droplets-gas co-flow is not fully developed. The number of fluid droplets is less in the center of the flow. As a result, the resulting film becomes thin and uneven. Also the interface did not receive sufficient cooling and lubrication effect, and hence accelerated tool wear and degraded surface finish.

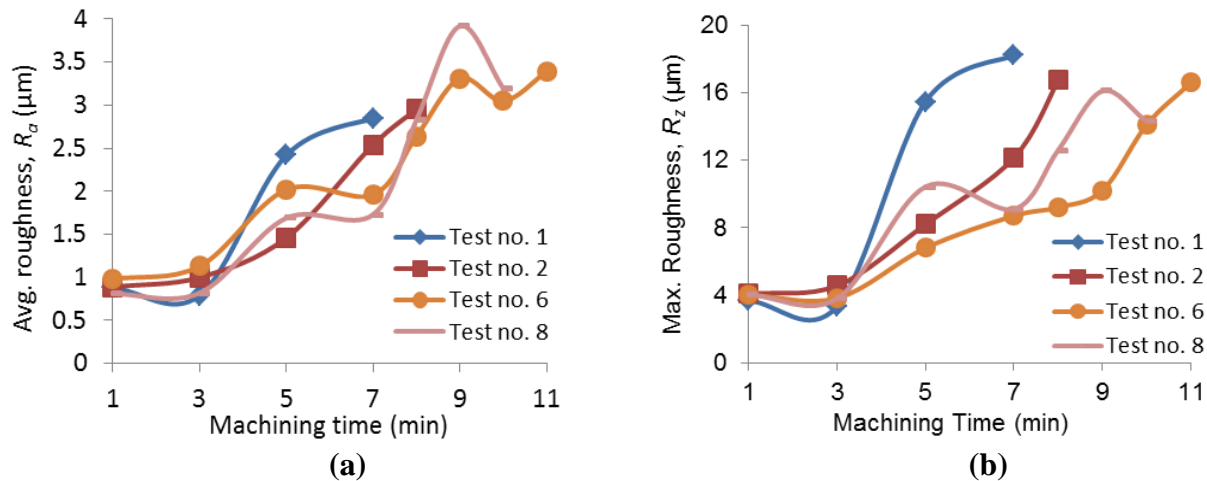


Figure – 11 (a) Average surface roughness, R_a ; and (b) maximum surface roughness, R_z values at different machining times for different spray conditions.

Table – 3 Cutting forces for various tests at different cutting intervals during turning of Ti-6Al-4V.

Test no.	Forces (N)	Machining time (min)							
		1	3	5	7	8	9	10	11
1	Thrust (F_x)	125.81	133.50	357.58	771.68				
	Feed (F_y)	136.66	149.45	348.21	592.23				
	Tangential (F_z)	437.17	455.34	572.72	685.63				
	Resultant	475.01	497.49	759.69	1190.09				
2	Thrust (F_x)	126.95	128.82	173.39	331.58	971.54			
	Feed (F_y)	138.42	140.73	155.46	396.13	886.08			
	Tangential (F_z)	428.55	443.13	457.88	554.42	751.57			
	Resultant	467.90	442.45	513.70	757.79	1502.95			
6	Thrust (F_x)	126.52	135.02	191.64	198.26	205.71	228.68	264.13	297.21
	Feed (F_y)	131.68	168.34	193.10	200.2	210.03	207.45	224.09	278.12
	Tangential (F_z)	430.97	462.22	481.93	503.65	524.67	520.00	541.40	596.60
	Resultant	468.06	510.12	553.42	577.10	601.42	604.76	642.72	722.23
8	Thrust (F_x)	106.70	157.88	236.21	278.05	390.71	444.47	447.56	
	Feed (F_y)	125.27	215.94	243.57	275.36	343.56	439.73	464.63	
	Tangential (F_z)	426.70	442.11	534.82	556.20	597.32	649.87	680.72	
	Resultant	457.33	516.74	633.37	680.07	792.14	901.80	937.86	

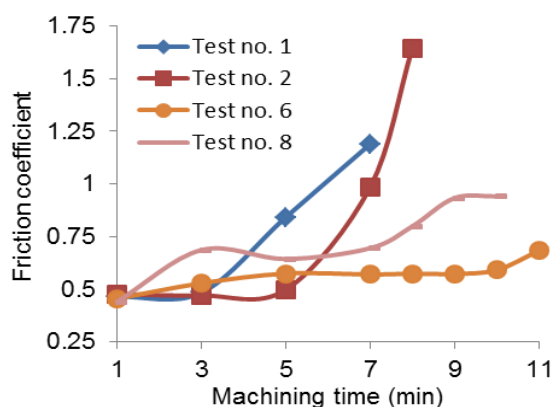


Figure – 12 Friction coefficient values at different machining times for different ACF spray conditions.

The effect of droplet velocity on the cutting forces and the friction coefficient can also be seen in Table 3 and Fig. 12, respectively, when comparing Test nos. 1 and 2. If the droplets are pushed from behind the atomizer tip (Fig. 1) at a higher velocity of 1.2 m/s compared to 0.2 m/s, these performances are found to be improved. This is due to the following reason. With the increase in droplet velocity, the droplet entrainment angle decreases (Eqn. (3)), which allows gradual development of the droplets and the gas and helps in avoiding droplet condensation effect (see Section 3). As a result, the cutting interface receives an effective cooling and lubrication effect, and therefore results in lower cutting force and friction coefficient.

When comparing Test nos. 6 and 8 for studying the effect of gas velocity, it is observed that a lower gas velocity offers lower cutting force and a smaller friction coefficient, as depicted in

Table 3 and Fig. 12. As seen in ACF spray experiment in Figs. 2(a)-(d), when gas velocity decreases, the droplet entrainment angle also decreases that again helps in obtaining lower cutting forces and lower friction coefficient.

It is interestingly observed that both the values of cutting force and friction coefficient appear to be close in first few minutes of cutting, say, 2-4 min. However, as the cutting progresses, the tool wear behavior changes, which responds to cutting forces and friction coefficient accordingly. It is because, in the beginning of cutting, a fresh tool can survive for some time with smaller increase in cutting force and friction coefficient values. However, the tool-chip cutting interface after 2-4 min suffers from immense rise in cutting temperature and friction. Thus, it continuously requires effective cooling and lubrication effect for protecting the tool wear. The study reveals that the lowest cutting force and friction coefficient can be achieved by setting a larger spray distance (35 mm), a higher droplet density (1.2 m/s), and a lower gas velocity (26 m/s).

5. CONCLUSIONS

Droplet spray characteristics of an atomization-based cutting fluid (ACF) system were experimentally and theoretically studied with respect to three ACF spray parameters including droplet and gas velocities, and spray distance. Machining experiments on a titanium alloy, Ti-6Al-4V also are performed in order to understand the effect of the droplet spray behavior on the machining performances, viz., tool life/wear, and surface finish. The following conclusions are drawn from this study:

- i) When a high-velocity gas dispenses at in the center in a droplet-gas co-flow jet, the diffusion between the droplets and the gas is fully-developed after a certain distance depending on the ACF spray conditions. The

fluid droplets are found to be distributed uniformly across the jet flare;

- ii) A higher droplet velocity and a smaller gas velocity result in a gradual development of co-flow with a larger droplet entrainment angle and entrainment zone, an early development of the self-similarity state. On the other hand, a smaller droplet velocity and a higher velocity may lead to condensation of the fluid droplets because of a higher droplet density at a comparatively smaller jet radius;
- iii) With an increase in spray distance and droplet velocity, and a decrease in gas velocity, the flow is seen to be fully-developed (i.e. self-similar) and the droplets are found to be distributed uniformly across the jet flare. These help in reducing the cutting forces and friction coefficient with an effective cooling and improved lubrication, thereby improving the machining performances, viz., tool life and wear, and surface roughness during turning of Ti-6Al-4V.

ACKNOWLEDGEMENT

The authors would like to thankfully acknowledge the financial support of the *TechSolve, Inc.*, Cincinnati, OH for conducting this research.

REFERENCES

- [1] Ezugwu, E.O., Wang, Z.M., 1997, Titanium alloys and their machinability—a review, *Journal of Materials Processing Technology*, 68: 262-274.
- [2] Palanisamy, S., et al., 2009, Effects of coolant pressure on chip formation while turning Ti6Al4V alloy, *International Journal of Machine Tools and Manufacture*, 49: 739-743.
- [3] Hong, S.Y., Ding, Y., 2001, Cooling approaches and cutting temperatures in cryogenic machining of Ti-6Al-4V, *International Journal of Machine Tools and Manufacture*, 41: 1417-1437.
- [4] Venugopal, K.A., et al., 2007, Tool wear in cryogenic turning of Ti-6Al-4V alloy, *Cryogenics*, 47: 12-18.
- [5] Venugopal, K.A., et al., 2007, Growth of tool wear in turning of Ti-6Al-4V alloy under cryogenic cooling, *Wear*, 262: 1071-1078.
- [6] Ezugwu, E.O., et al., 2005, Evaluation of the performance of CBN tools when turning Ti-6Al-4V alloy with high pressure coolant supplies, *International Journal of Machine Tools and Manufacture*, 45: 1009-1014.
- [7] Nandy, A.K., et al., 2009, Some studies on high-pressure cooling in turning of Ti-6Al-4V, *International Journal of Machine Tools and Manufacture*, 49: 182-198.
- [8] Hong, S.Y., et al., 2001, New cooling approach and tool life improvement in cryogenic machining of titanium alloy Ti-6Al-4V, *International Journal of Machine Tools and Manufacture*, 41: 2245-2260.
- [9] Pusavec, F., et al., 2010, Transition to sustainable production—Part I: application on machining technologies, *Journal of Cleaner Production*, 18: 174-184.
- [10] Nath, C., Kapoor, S.G. DeVor, R.E., Srivastava, A.K., Design and evaluation of an atomization-based cutting fluid spray system in turning of titanium alloy, *In Proceedings of the NAMRI/SME*, Vol. 40, Notre Dame, Indiana, USA, 4-8 June, 2012.
- [11] Rukosuyev, M., et al., 2010, Understanding the effects of system parameters of an ultrasonic cutting fluid application system for micromachining, *Journal of Manufacturing Processes* 12: 92-98.
- [12] Rukosuyev, M., Goo, C.S., Jun, M.B.G, Park, S.S., 2010, Design and development of cutting fluid system based on ultrasonic atomization for micro-machining, *Transaction of the NAMRI/SME* 38: 97-104.
- [13] Jun, M.B.G., et al., 2008, An experimental evaluation of an atomization-based cutting fluid application system for micromachining, *ASME Transactions - Journal of Manufacturing Science and Engineering*, 130: 0311181-8.
- [14] Ghai, I., et al., 2010, Droplet behavior on a rotating surface for atomization-based cutting fluid application in micromachining, *ASME Transactions, Journal of Manufacturing Science and Engineering* 132: 011017-10.
- [15] Ghai, I., 2010, Analysis of droplet behavior on a rotating surface in atomization-based cutting fluid systems for micro-machining, MS Thesis, University of Illinois at Urbana-Champaign, Urbana, Illinois, USA.
- [16] Ricou, F.P., Spalding, D.B., 1961, Measurements of entrainment by axisymmetrical turbulent jets, *Journal of Fluid Mechanics* 11: 21-32.
- [17] Papadopoulos, G., Pitts, W.M., 1998, Scaling the near-field centerline mixing behavior of axisymmetric turbulent jets 36: 1635-1642.
- [18] Pitts, W.M., 1991, Reynolds number effects on the mixing behavior of axisymmetric turbulent jets, *Experiments in Fluids* 11: 135-141.
- [19] Pitts, W.M., 1991, Effects of global density ratio on the centerline mixing behavior of axisymmetric turbulent jets, *Experiments in Fluids* 11: 125-134.
- [20] Fellouah, H., Ball, C.G., Pollard, A., 2009, Reynolds number effects within the development region of a turbulent round free jet, *International Journal of Heat and Mass Transfer* 52: 3943-3954.
- [21] Parker, R., Rajagopalan, S., Antonia, R.A., 2003, Control of an axisymmetric jet using a passive ring, *Experimental Thermal and Fluid Science* 27: 545-552.
- [22] Rothe, P.H., Block, J.A., 1977, Aerodynamic behavior of liquid sprays, *International Journal of Multiphase Flow* 3: 263-272.
- [23] Lee, S.Y., Tankin, R.S., 1984, Study of liquid spray (water) in a non-condensable environment (air), *International Journal of Heat and Mass Transfer* 27: 351-361.
- [24] Bernoulli's Principle, http://en.wikipedia.org/wiki/Bernoulli_effect.
- [25] Maczyński, J.F.J, 1961, A round jet in an ambient co-axial stream, *Journal of Fluid Mechanics* 13: 597-608.
- [26] Jet flow, <http://encyclopedia2.thefreedictionary.com/Jet+Flow>.